Effectiveness of Emission Controls on Atmospheric Oxidation and Air Pollutant Concentrations: Uncertainties due to Chemical Mechanisms and Inventories

Mingjie Kang[1,2], Hongliang Zhang[3], Qi Ying[4,a]

[1] School of Applied Meteorology, Nanjing University of Information Science and Technology. Nanjing 210044, China.

[2] Atmospheric Environment Center, Joint Laboratory for International Cooperation on Climate and Environmental Change, Ministry of Education, Nanjing University of Information Science and Technology. Nanjing 210044, China.

[3] Department of Environmental Science and Engineering, Fudan University, Shanghai 200433, China.

[4] Zachry Department of Civil and Environmental Engineering, Texas A&M University, College Station, Texas 77843-3136, USA.

[a] Currently at the Division of Environment and Sustainability, Hong Kong University of Science and Technology, Clear Water Bay, Kowloon, Hong Kong, China.

Correspondence to: Qi Ying (qying@ust.hk)

Abstract. In this study, three photochemical mechanisms of varying complexity from the Statewide Air Pollution Research Center (SAPRC) family and two widely used anthropogenic emission inventories are employed to quantify the discrepancies in the predicted effectiveness of nitrogen oxides (NO_x) and volatile organic compound (VOC) emission controls on ozone (O_3), secondary inorganic aerosols (SIA), and hydroxyl (OH) and nitrate (NO_3) radicals using the Community Multiscale Air Quality (CMAQ) model. For maximum daily average 8-hour O_3 (O_3-8h), relative reductions predicted using different emission inventory and mechanism combinations are consistent for up to 80% NO_x or VOC reductions, with maximum differences of approximately 15%. For SIA, while the predicted relative changes in their daily average concentrations due to NO_x reductions are quite similar, very large differences of up to 30% occur for VOC reductions. Sometimes even the direction of change (i.e., increase or decrease) is different. For the oxidants OH and NO_3 radicals, the uncertainties in the relative changes due to emission changes are even larger among different inventory-mechanism combinations, sometimes by as much as 200%. Our results suggest that while the O_3-8h responses to emission changes are not sensitive to the choice of chemical mechanism and emission inventories, using a single model and mechanism to evaluate the effectiveness of emission controls on SIA and atmospheric oxidation capacity may have large errors. For these species, the evaluation of the control strategies may require an ensemble approach with multiple inventories and mechanisms.

1. Introduction

Tropospheric ozone (O_3) pollution remains a major global concern. O_3 plays a critical role in atmospheric chemistry and is an important target for air quality improvement (Lu et al., 2018; Lyu et al., 2023; Real et al., 2024) because high levels of surface O_3 negatively affect human health, agricultural crop yields and plant growth (Du et al., 2024; Feng et al., 2022; Ghude et al., 2016; Lu et al., 2020; West et al., 2006). Surface O_3 is mainly formed by the photochemical reactions of NO_x and volatile organic compounds (VOCs) emitted from anthropogenic and biogenic sources (Finlayson-Pitts and Pitts Jr, 1999; Seinfeld and Pandis, 2016). The development of effective O_3 control strategies is hampered by the considerable spatial and temporal variability of surface O_3 concentrations and their non-linear relationship with emissions and meteorological conditions.

Three-dimensional chemical transport models (CTMs) are a valuable tool for developing effective air pollution control strategies. They can provide spatial and temporal information on O_3, particulate matter, and toxic air pollutants by numerically solving the mathematical equations describing the emission, reaction, transport, and deposition of primary and secondary atmospheric pollutants (Byun and Schere, 2006; Russell, 1997). The veracity of modeling outcomes is contingent upon the gas-phase chemical mechanisms and emission inventories, among other variables. Reliance on a single chemical mechanism and emission inventory may result in substantial uncertainty in modelled pollutant concentrations. A common approach to reduce uncertainty in air quality model predictions is to use an ensemble of simulations with different emission inventories and chemical mechanisms (Hu et al., 2017a).

Photochemical mechanism is one of the core components of all CTMs. While the representation of inorganic chemistry is generally similar across mechanisms, the representation of atmospheric organic chemistry differs significantly in terms of the number of explicit model species, the lumping schemes, and the radical chemistry, leading to variations in the model predictions of O_3, $PM_{2.5}$, air toxics, and some important radical species (Griffith et al., 2016; Kim et al., 2009). Furthermore, the responses of the predictions to changes in emissions may also differ depending on the photochemical mechanism employed, which may impact the assessment of emission control strategies. In practical applications, it is of the utmost importance to strike a balance between mechanism complexity and computational efficiency. For long-term modeling studies of criteria pollutants and the evaluation of numerous emission control strategies, condensed mechanisms may prove to be the optimal choice. More detailed mechanisms are appropriate for a broader range of applications, such as

71 investigations into specific reaction products that are not explicitly represented in condensed

72 mechanisms. However, they are more demanding on computational resources.

73   In this context, several mechanism comparison studies have been conducted. Differences

74 in predicted O_3 levels using various photochemical mechanisms have been reported (Yu et al.,

75 2010; Venecek et al., 2018). In addition to directly comparing the model predictions of O_3

76 concentrations, comparative analyses were also undertaken to examine the similarities and

77 differences between these mechanisms in predicting O_3 changes in response to changes in

78 precursor emissions. For example, Li et al. (2012) and Kang et al. (2022) compared several

79 mechanisms from the SAPRC family, including the standard versions of SAPRC-99, SAPRC-

80 07, SAPRC-11, and a highly condensed version of SAPRC-07. Their results showed that,

81 despite discrepancies in the predictions for O_3, key radicals such as OH and HO_2, and oxidation

82 products such as HNO_3, H_2O_2, NO_2, PAN, and HCHO, the relative changes in O_3 due to

83 changes in NO_x and VOC emissions were almost identical.

84   On the other hand, the accuracy of model predictions is also significantly affected by

85 uncertainties in anthropogenic emission inventories (Hu et al., 2017a; Kang et al., 2022; Placet

86 et al., 2000), which primarily arise from uncertainties and variability in activity levels (e.g.,

87 industrial production or energy consumption) and emission factors (Akimoto et al., 2006; Lei

88 et al., 2011; Streets et al., 2003). For example, when local speciation profiles are not available

89 for the generation of mechanism-specific VOC emissions from the emission rate of non-

90 methane hydrocarbons, average speciation profiles from the SPECIATE database developed

91 by the US EPA were often adopted (Bray et al., 2019; Li et al., 2014; Streets et al., 2003; Wu

92 and Xie, 2017). However, the emission factors from the SPECIATE profiles are predominantly

93 representative of the characteristics of local emissions, as a consequence of the disparities in

94 emission standards and control technologies among diverse geographical regions (Sha et al.,

95 2021). This introduces uncertainties into the emissions and the predicted pollutant

96 concentrations.

97   To date, several emission inventories covering China have been developed, such as the

98 Multi-resolution Emission Inventory for China (MEIC), the Regional Emission inventory in

99 ASia (REAS), and the Emission Database for Global Atmospheric Research (EDGAR). These

100 inventories have been successfully applied in chemical transport modeling to investigate the

101 concentration and spatial distribution of O_3 and other pollutants (Hu et al., 2017b; Kang et al.,

102 2021; Li et al., 2019, 2018; Saikawa et al., 2017; Xue et al., 2020; Yamaji et al., 2008). Hu et

103 al. (2017a) reported inconsistencies in emission inventories in predicting O_3 and $PM_{2.5}$ using

104 the Weather Research and Forecasting/Community Multiscale Air Quality (WRF/CMAQ)

model system. Ma et al. (2004) identified variations in NO_x and VOC emissions among different inventories as the main factors influencing modeled O_3 concentrations. Our previous study, which employed the condensed SAPRC-07 mechanism and two anthropogenic emission inventories (MEIC and REAS), also observed relatively larger differences in O_3 predictions between inventories in megacities of Beijing and Shanghai, especially on days with elevated O_3 levels (Kang et al., 2022).

While several studies have explored the differences in model predictions due to varying chemical mechanisms or emission inventories, a comprehensive analysis of the influence of diverse combinations of these two factors on the sensitivity of O_3 and other air pollutants to emission changes in China has yet to be undertaken. In this study, we address this gap by applying the CMAQ model, integrated with three photochemical mechanisms and two widely used emission inventories, to quantify the effects of different combinations of mechanisms and inventories on the predictions of maximum daily average 8-hour ozone (O_3-8h) and other secondary pollutants in different regions of China. In addition, the impacts on atmospheric oxidation capacity and key gaseous pollutants are investigated. To gain insight into the variations in pollutant sensitivity, a series of incremental emission reduction scenarios were used, thereby enabling the quantification of the influence of different mechanism and inventory combinations on the response of O_3 and related pollutants. The findings of this study can assist policymakers in the development of more effective and adaptive pollution control strategies.

2. Materials and methods

2.1 The CS07, SAPRC-11 and SAPRC-18 mechanisms

The SAPRC mechanism is a widely used photochemical mechanism that represents complex atmospheric reactions in computationally tractable forms. Instead of tracking the oxidation of individual precursor organic compounds and their reaction products explicitly, the SAPRC is a lumped-molecule chemical mechanism that groups structurally similar VOC species (e.g., alkanes, akenes, and aromatics) into several groups of lumped model species. Some important species, such as isoprene and formaldehyde, are represented explicitly. The reactions of each lumped model species with common oxidants (OH, NO_3 and O_3) are derived based on the reactions of individual species within that group, which are generated automatically using a mechanism generator (Carter et al., 2025). One of the complexities in representing VOC reactions is the intermediate oxidation products and radical species. In the SAPRC mechanism, the radicals such as peroxyl radicals and intermediate products such as organic nitrates are

138 represented by a group of common species to reduce the number of reactions and model species.

139 A brief comparison of the three SAPRC mechanisms is summarized in Table S1.

140 Three different chemical mechanisms from the SAPRC mechanism family were used in

141 this study, i.e., the condensed SAPRC-07 (CS07) (Carter, 2010), the standard SAPRC-11 (S11)

142 (Carter and Heo, 2013), and the standard SAPRC-18 (S18) (Carter, 2020). These mechanisms

143 were selected to represent different levels of detail in gas-phase reactions in a regional chemical

144 transport model. The CS07 was derived from the widely used SAPRC-07 mechanism and has

145 a high condensation level similar to that of the Carbon Bond mechanism, which is also widely

146 used. The S11 is an updated version of the SAPRC-07 mechanism, with significant revisions

147 made to the aromatic chemistry. The S11 mechanism employed in this study is identical to that

148 utilized in our previous study (Kang et al., 2021). For a detailed description of CS07 and S11

149 regarding O_3 source apportionment and emission sensitivity, please refer to Kang et al. (2022).

150 The S18 mechanism represents a complete update of the SAPRC mechanism since SAPRC-07.

151 S18 incorporates a greater number of model species, a more explicit representation of peroxyl

152 radical chemistry, and a lumping scheme that is more suitable for predicting secondary organic

153 aerosol (SOA) formation. Due to these modifications, S18 is more extensive than S11 in terms

154 of both the number of species and chemical reactions. Although it has been successfully applied

155 in photochemical box models (Jiang et al., 2020; Li et al., 2022a, b), it has not yet been

156 implemented in 3D regional CTMs.

157

158 **2.2. Anthropogenic emission inventories**

159 The present study compares two widely used anthropogenic emission inventories, MEIC

160 (http://www.meicmodel.org) and REAS 3.1 (https://www.nies.go.jp/REAS/), to investigate O_3

161 pollution in China. The emission data from these inventories were processed using an in-house

162 emission processor. Detailed VOC speciation profiles selected from the US EPA-developed

163 SPECIATE database were processed using the speciation profile processor from W.P.L. Carter

164 (2015) to generate profiles for the CS07, SAPRC-11, and SAPRC-18 mechanisms, which are

165 used to estimate emissions of CMAQ-ready VOCs. The MEIC emission inventory includes

166 only emission estimates in China, whereas the REAS emission inventory has complete spatial

167 coverage for Asian countries. In the MEIC simulation, emissions from other countries are

168 supplemented using data from the REAS inventory.

169

170 **2.3 Model application**

The CS07, S11, and S18 mechanisms were incorporated into the CMAQ model (version 5.0.2) to evaluate the differences of mechanisms and inventories in predicting O_3-8h, OH and NO_3 radicals, secondary inorganic aerosols, and reactive VOC species (HCHO) in July 2017 in China. July is widely used in modeling studies to represent conditions of a typical summer month (Kang et al., 2021). The model domain, which covers China and surrounding areas in eastern and southeastern Asia at a 36 km × 36 km horizontal resolution, along with the locations of cities mentioned in the manuscript, is illustrated in Figure S1.

The simulations included model runs with the following combinations: S11 mechanism with MEIC inventory (S11-MEIC), S11 with REAS (S11-REAS), CS07 with MEIC (CS07-MEIC), CS07 with REAS (CS07-REAS), and S18 with REAS (S18-REAS). The MEIC only has five emission sectors, making it difficult to re-speciate the emissions for the S18 mechanism. Specifically, solvent utilization emissions are not represented in the public version of MEIC as a separate sector (Wang et al., 2018). Since solvent utilization accounts for a significant fraction of VOC emissions in urban areas and has very different emission characteristics than fuel combustion sources, re-speciating the five-sector MEIC VOC emissions will be inaccurate. It should be noted that while the MEIC emission inventory is for 2017, the most recent year in the REAS inventory is 2015, which is the one used in the current study.

The July anthropogenic emission inventories from MEIC and REAS were processed using an in-house emission processor, with updated speciation profiles employed to generate CMAQ-ready VOC emissions (Kang et al., 2022). The speciation profiles for different chemical mechanisms were derived from the same detailed speciation profiles extracted from the SPECIATE database. Comprehensive overviews of MEIC and REAS inventories were provided by Kang et al. (2022). Comparisons of major species, including NO_x ($NO+NO_2$), SO_2, ethene (ETHENE), formaldehyde (HCHO), higher olefins (OLE) (comprising OLE1 and OLE2, which are lumped alkene species with propylene and trans-2-pentene as representative compounds), isoprene (ISOPRENE), and monoterpenes (TRP1), are shown in Tables S2-S3 and Figures S2-S3 for municipalities and provinces in July 2017. Note that OLE and TRP1 emissions are from the S11 mechanisms. Emissions for CS07 are similar but some of the species in OLE and TRP1 are explicit species in S18. There are notable spatial differences in the weekday emissions of HCHO, ETHENE, OLE, SO_2, and NO_x between MEIC and REAS. Specifically, REAS exhibits higher HCHO emissions in locations like Beijing, Tianjin, Henan, Shanghai, and Guangzhou than MEIC (Figure S2). In the south of Henan, ethene emissions are

significantly higher in REAS relative to MEIC. The emissions of OLE in REAS are lower than those in MEIC in Beijing, Tianjin, Shanghai, Guangzhou, Chengdu, and Chongqing. SO_2 emissions in MEIC are generally lower than those in REAS, except for Shanghai and Guangzhou. NO_x emissions differ significantly between MEIC and REAS. In eastern China, including cities like Shanghai and Guangzhou, NO_x emissions from REAS are typically lower than those from MEIC, although some areas demonstrate a notable increase. These discrepancies inevitably affect the accuracy of air pollutant predictions, underscoring the necessity for a comprehensive assessment of emission inventories in the development of effective pollution control policies.

Biogenic emissions were generated using the Model of Emissions of Gases and Aerosols from Nature (MEGAN) version 2.10, which has been observed to emit higher levels of isoprene and monoterpenes in comparison to anthropogenic sources (Figure S3). Open burning emissions were produced using FINN inventory from the National Center for Atmospheric Research (NCAR) (Wiedinmyer et al., 2011). Sea salt and windblown dust emissions were simulated online using the CMAQ model. Initial and boundary conditions for the model simulation were generated using CMAQ default profiles. The initial three days of the simulation serve as a spin-up and are excluded from subsequent analyses.

Meteorological inputs were generated using the Weather Research and Forecasting (WRF) model version 4.2 for the 36×36 km domain with 44 vertical layers. The initial and boundary conditions for WRF were derived from the global reanalysis data FNL (available at https://rda.ucar.edu/datasets/ds083.2/). Further details on the configuration of WRF model can be found in the work of Kang et al. (2022). WRF-derived meteorological parameters, including temperature and relative humidity at a height of 2 m above the surface and wind speed and direction at 10 m, have been validated against observational data from the National Climatic Data Center (NCDC), demonstrating good performance (Kang et al., 2021).

2.4 Sensitivity of O_3 and related pollutants to emission controls across different mechanisms and inventories

A large number of sensitivity simulations with systematic reductions in NO_x and VOC emissions were conducted to explore variations in the sensitivity of O_3-8h and related pollutants to emission reductions across different mechanisms and inventories. Three sets of simulations were performed for each mechanism/inventory combination considered in this study (see section 2.3). In the first set of simulations, NO_x emissions were reduced by 20, 40,

237   50, 60, and 80%, while the emissions of VOCs were maintained at their base-case level. In the

238   second set of simulations, VOC emissions were reduced by 20, 40, 50, 60, and 80%, while NO_x

239   emissions remained constant. In the third set of simulations, both NO_x and VOC emissions

240   were reduced by 20, 40, 50, 60, and 80%.

241

242   **3. Results and discussion**

243   **3.1 Model evaluation of O_3 and $PM_{2.5}$ predictions across various mechanisms and**

244   **inventories**

245   Observations of O_3-8h and $PM_{2.5}$ at a large number of surface monitoring stations nationwide

246   in July 2017 were obtained from the publication website of the China National Environmental

247   Monitoring Center (http://www.cnemc.cn). The model performance statistics were evaluated

248   separately for different regions: the North China Plain (NCP), Yangtze River Delta (YRD),

249   Central China (Center), Pearl River Delta (PRD), and Sichuan Basin (SCB). Specifically, NCP

250   includes Beijing, Tianjin, and some cities in Hebei and Shandong provinces; Center includes

251   cities in the provinces of Henan, Hubei, Hunan, and Jiangxi; YRD includes Shanghai and some

252   cities in the provinces of Anhui, Jiangsu, and Zhejiang; PRD includes Shenzhen and some

253   cities in Guangdong province; and SCB includes Chongqing and some cities in Sichuan

254   province. As shown in Figures S4-S5, the model performance for O_3-8h and $PM_{2.5}$ predicted

255   by different mechanisms and emission inventories in major regions of China exhibits large

256   variations, due to differences in climate, topography, and emission sources. Overall, the

257   average values of mean normalized bias (MNB) and mean normalized error (MNE) for O_3-8h

258   predictions across all combinations of mechanisms and inventories are generally within the

259   recommended model performance criteria (MNB≤±0.15 and MNE≤0.3) (Emery et al., 2017)

260   in most regions, except for underprediction in the PRD. Similarly, the model shows good

261   performance for $PM_{2.5}$ in most areas, except for the PRD region, where the mean fractional

262   biases (MFB) for $PM_{2.5}$ using S18-REAS, CS07-REAS, and S11-REAS are slightly outside

263   the recommended range (Boylan and Russell, 2006). The underestimation of $PM_{2.5}$ predictions

264   using REAS in the PRD, as shown in Figure S5, is likely related to biases in this inventory

265   specific to this region.

266

267   **3.2 Spatial variations in predictions of O_3 and related pollutants by different mechanisms**

268   **and inventories**

269   Figure 1 shows the spatial distribution of monthly averaged O_3-8h concentrations predicted by

270   S11-MEIC in July, along with the absolute differences between O_3-8h predictions from S11-

271   MEIC and those from other mechanisms and inventories. Based on S11-MEIC, high O_3-8h

272   levels exceeding 80 ppb occurred in eastern China, especially in Beijing, Tianjin, Hebei,

273   northern Henan, SCB, and Shanghai. Extremely high O_3-8h levels above 100 ppb are also

274   observed over the Bohai Bay and the Yellow Sea, likely due to regional transport of polluted

275   air from the continent, reduced NO_x titration with O_3, and lower O_3 dry deposition velocities

276   over the ocean (Luhar et al., 2017; Silva and Heald, 2018). Similar spatial distributions of O_3-

277   8h concentrations are also found in the simulations using other mechanisms and inventories

278   (Figure S6). In comparison, O_3-8h concentrations predicted by S11-REAS are generally 2–7

279   ppb higher than those by S11-MEIC in most parts of China, especially in the central region,

280   Zhejiang, and Fujian provinces, but about 2–7 ppb lower in Beijing, Shanghai, Chengdu, and

281   the PRD region. S18-REAS predicted significantly lower O_3-8h levels, with reductions greater

282   than 7 ppb in regions such as Beijing, Tianjin, Hebei, Shanghai, SCB, PRD, and other

283   developed areas such as Zhengzhou and Hefei.

284   In contrast, CS07-MEIC predicted lower O_3-8h levels overall, with apparent reductions of

285   ~ 6–7 ppb in the SCB, central China, and coastal areas near Shanghai. Similarly, CS07-REAS

286   also showed generally lower O_3-8h concentrations compared to S11-MEIC, particularly in

287   Chengdu, Luoyang, Shanghai, Guangzhou, Ningbo, Hefei, Nanchang, and the Yellow Sea (~7

288   ppb lower or more), although some locations exhibit higher O_3-8h levels than those predicted

289   by S11-MEIC. These discrepancies highlight that the accuracy of O_3 predictions is sensitive to

290   variations in photochemical mechanisms and emission inventories. This underscores the

291   importance of adopting and comparing multiple mechanisms and inventories when developing

292   region-specific pollution control policies.

293   The difference in Figure 1(c) for other countries is mainly due to the difference between

294   S11 and S18. Predicted O_3 concentrations by S18 are lower than those by S11, especially in

295   urban areas (e.g., in Ulaanbaatar in Mongolia). This is consistent with the box-model

296   simulation results reported by Carter (Carter, 2020). In Figure 1(a), the difference of the

297   monthly O_3 in other countries is negligible when the same chemical mechanism is used,

298   which further confirms our conclusion.

299   In Figures 1(b), O_3 concentrations from S11-REAS are significantly lower than those

300   from S11-MEIC. This is because O_3 formation sensitivity regime over the yellow sea is likely

301   NO_x-limited as the VOC-sensitive urban plume is advected to the marine environment

302   (Vermeuel et al., 2019). Furthermore, satellite observed $HCHO/NO_x$ columns over the

303   Yellow Sea is greater than 6, clearly indicating a NO_x-limit regime (Kang et al., 2021). Since

304   the NO_x emissions in the upwind regions in the REAS inventory are significantly lower than

305 these in the MEIC inventory, this leads to reduced O_3 formation in the S11-REAS results

306 compared to the S11-MEIC results.

307   Figure 2 illustrates the differences in spatial distribution of monthly averaged secondary

308 inorganic aerosol (SIA) concentrations modeled with different mechanisms and inventories.

309 According to S11-MEIC, high SIA concentrations are mainly concentrated in NCP and SCB,

310 exceeding 15 μg m^{-3}. High SIA concentrations are also found in Bohai Bay, likely due to long-

311 range transport of polluted air from land sources. Compared to S11-MEIC, S11-REAS predicts

312 higher SIA concentrations in most regions, with increases of > 1 μg m^{-3} in most areas,

313 especially in NCP, Henan, and SCB (higher by about 6 μg m^{-3} or even more). Nationwide, SIA

314 concentrations predicted by S18-REAS are generally higher than those predicted by S11-MEIC,

315 with increases of up to 6 μg m^{-3} or more in the NCP, Central China, SCB, Bohai Bay, and the

316 Yellow Sea. CS07-MEIC shows similar SIA levels to S11-MEIC, with slightly lower

317 concentrations of ~1 μg m^{-3} in SCB and Bohai Bay. The spatial differences in SIA predictions

318 between CS07-REAS and S11-MEIC are similar to those between S11-REAS and S11-MEIC,

319 suggesting that SIA concentrations from CS07-REAS and S11-REAS are comparable.

320

321 3.3 Impacts of mechanisms and inventories on predicted atmospheric oxidation capacity

322 Atmospheric oxidation capacity (AOC), which governs the removal rate of primary pollutants

323 and the production of secondary pollutants (Elshorbany et al., 2009; Prinn, 2003), is primarily

324 controlled by the hydroxyl (OH) and nitrate (NO_3) radicals in the atmosphere (Geyer et al.,

325 2001; Liu et al., 2022). The spatial differences in OH and NO_3 predictions for different

326 mechanisms and inventories are illustrated in Figures 3-4.

327   S11-MEIC predicts high OH concentrations exceeding 3.7×10^6 molecules cm^{-3} (0.15 ppt)

328 mainly in northern China, including NCP, Inner Mongolia, and some western sites. Compared

329 to S11-MEIC, S11-REAS predicts lower OH concentrations in NCP, Jiangsu, Shanghai, PRD,

330 SCB, and other urban nuclei but higher concentrations in rural areas. In contrast, S18-REAS

331 predicts higher OH concentrations than S11-MEIC in most regions, except in some northern

332 locations. CS07-MEIC produces elevated OH concentrations in northwestern China, Chengdu,

333 Chongqing, Shanghai, Hebei, Shandong, and northern Henan, but lower OH levels in other

334 regions. Similar to S11-REAS, CS07-REAS shows much higher OH levels in northwestern

335 China but lower OH levels in eastern regions than S11-MEIC. The variability in OH levels can

336 significantly affect the formation of O_3 and other gaseous and particulate pollutants.

The spatial distribution of NO_3 concentrations modeled by S11-MEIC exhibits high values in Xinjiang, Inner Mongolia, NCP, and Bohai Bay, with NO_3 concentrations reaching up to 20 ppt. Obvious differences in NO_3 predictions between S11-REAS and S11-MEIC are primarily observed in Xinjiang and Inner Mongolia, with smaller differences in other regions. S18-REAS generally predicted higher NO_3 concentrations than S11-MEIC, especially in Xinjiang, Inner Mongolia, Bohai Bay, Yellow Sea, and Taiwan Strait, by ~6 ppt or more. In contrast, CS07-MEIC consistently predicts lower NO_3 levels than S11-MEIC. CS07-REAS predicted lower NO_3 concentrations in the eastern regions but higher concentrations in parts of Xinjiang compared to S11-MEIC.

3.4 Impacts of mechanisms and inventories on HCHO prediction

Spatial variations in AOC, as reflected in OH and NO_3 predictions from different mechanisms and inventories, imply that photochemical formation and loss rates for air toxics may also vary depending on the mechanism and inventory used. To explore how these variations affect the modeling results for gaseous pollutants, we examined HCHO, one of the most important gaseous air toxics with both primary and secondary sources. It is also a significant contributor to O_3 formation and OH production, thus playing a crucial role in tropospheric photochemistry (Wang et al., 2017; Zhang et al., 2013).

Monthly average surface HCHO concentrations from S11-MEIC are similar to the surface observations made in China (Zhang et al., 2021). HCHO concentrations are generally high in the SCB and eastern China, areas with significant biogenic VOC emissions (Kang et al., 2023a), particularly in Chengdu, Shanghai, and Changsha, where HCHO concentrations reach or exceed 7 ppb (Figure 5). This suggests that a significant fraction of the HCHO is due to secondary formation. HCHO levels predicted by S11-REAS are similar to those predicted by S11-MEIC, with only minor differences of less than 1 ppb. In contrast, S18-REAS predicts significantly lower HCHO levels than S11-MEIC, with differences > 1 ppb, especially in SCB, NCP, PRD, YRD, and central China. CS07-MEIC and CS07-REAS predict higher HCHO levels than S11-MEIC, especially in SCB and eastern China, with differences exceeding 1 ppb. These results indicate that HCHO predictions are more strongly influenced by photochemical mechanisms than by uncertainties in emission inventories, due to its secondary formation.

3.5 Impacts of mechanisms and inventories on the sensitivity of O_3 and related pollutants to emission controls

370   Figures 6-10 and S6-S15 display the fractional changes in predictions of O_3 and related

371   pollutants due to NO_x and VOC reductions using various mechanisms and inventories.

372   **3.5.1 Impacts of mechanisms and inventories on O_3 sensitivity to emission controls**

373   For all mechanisms and inventories, O_3-8h concentrations consistently decrease with

374   reductions in NO_x, VOCs, or both in all five cities in July. The efficiency of emission controls

375   improves with increasingly higher emission reductions of NO_x, VOCs. These trends are

376   consistent with the findings of Kang et al. (2021), suggesting that the mechanisms and

377   inventories do not affect the trend of change in O_3, but do affect the magnitude of the change.

378   These results also show that in July, the sensitivity of O_3 formation to NO_x and VOCs is in

379   transition or NO_x-limited regimes. In Beijing, when NO_x emissions are reduced, CS07-MEIC

380   and CS07-REAS show the largest O_3-8h reductions compared to other mechanisms and

381   inventories, while S18-REAS exhibits the smallest changes, especially with larger NO_x

382   reductions. In Shanghai, the largest O_3-8h reductions due to NO_x controls are observed with

383   CS07-REAS, followed by S11-REAS, while S18-REAS again shows the smallest changes. In

384   Changsha, there are no significant differences among mechanisms and inventories in the

385   sensitivity tests. In Shenzhen, S11-REAS shows the greatest decreases in O_3-8h, followed by

386   CS07-REAS and S18-REAS, while S11-MEIC and CS07-MEIC show the smallest changes.

387   Except for S18-REAS, predictions from other mechanisms and inventories are similar in

388   Chongqing.

389   When only VOC emissions are reduced in Beijing, S11-MEIC predicts the largest O_3-8h

390   reductions, while CS07-REAS predicts the smallest changes. Similar patterns are found in

391   Shanghai and Changsha, with larger differences among different mechanisms and inventories

392   in Shanghai. In Shenzhen, S11-MEIC also exhibits the largest O_3-8h decreases, followed by

393   CS07-MEIC, while CS07-REAS, S11-REAS, and S18-REAS show smaller changes. In

394   Chongqing, S18-REAS predicts the largest changes and CS07-MEIC the smallest, although

395   the differences among these scenarios are not substantial. When both NO_x and VOC emissions

396   are reduced, the predicted change rates of O_3-8h do not vary much across different mechanisms

397   and emission inventories for all five cities. Additionally, the sensitivity tests for Shenzhen, as

398   presented in Figure 6, suggest that differences in emission inventories may have a greater

399   impact on emission control outcomes than differences in chemical mechanisms. O_3 in

400   Shenzhen is lower than other cities included in Figure 6 and most O_3 there is background O_3

401   on typical days (Kang et al., 2023b). Thus, it is less responsive to emission reductions than

402   other cities.

Figure S6 illustrates the national-scale relative changes in O_3-8h due to NO_x emission reductions evaluated using different mechanisms and inventories. The results are consistent with those shown in Figure 6, with the greatest O_3-8h reductions occurring in the SCB, Central, and YRD. For all mechanisms and inventories, increasingly higher NO_x reductions generally lead to increasingly lower O_3 in July, with relative changes in O_3-8h ranging from approximately 5% to 60% as NO_x reductions increase from 20% to 80%. In comparison, the O_3-8h reductions predicted by S18-REAS are less pronounced than other mechanisms and inventories in most areas. Similar to NO_x reductions, higher VOC reductions typically result in larger O_3 reductions in July, with significant reductions observed in NCP, Chengdu, PRD, Shanghai, and Bohai Bay. The relative changes in O_3-8h increase from 5% to 40% as VOC reductions increase from 20% to 80% in these areas (Figure S7). The comparison between Figure S6 and Figure S7 suggests that NO_x reduction tends to be more effective in controlling O_3 pollution in non-VOC-limited regions than VOC reduction, given the same level of emission reduction.

3.5.2 Impacts of mechanisms and inventories on SIA sensitivity to emission controls

Reducing NO_x emissions typically leads to decreasing SIA levels across the five cities, with the efficiency of reductions improving as NO_x reduction increases. As illustrated in Figure 7, the predicted changes in SIA are quite similar for different mechanisms and inventories. However, VOC controls do not always effectively reduce SIA concentrations, likely attributable to an increase in NO_3 radicals, as shown in Figure 9. In Beijing, changes in SIA in response to VOC reductions vary with mechanisms and inventories. For S11-MEIC and CS07-MEIC, SIA concentration first increases and then decreases with decreasing VOCs. S18-REAS shows a general decrease in SIA concentrations with decreasing VOCs. In contrast, CS07-REAS and S11-REAS predict an increase in SIA concentrations with VOC reductions, with the rate of SIA growth initially increasing and then decreasing as VOC emission decreases. In Shanghai, VOC reductions generally increase SIA concentrations across all mechanisms and inventories, especially for CS07-REAS and S11-REAS, which show that SIA concentrations consistently increase as VOCs are progressively reduced. In Changsha, SIA concentrations also consistently increase with increasing VOC reductions for all mechanisms and inventories. In Shenzhen, SIA concentrations increase with VOC reductions; however, the changes are more pronounced for S11-REAS compared to the less significant variations observed for CS07-MEIC. Except for S18-REAS, Chongqing shows an increase in SIA concentrations with VOC

reductions, particularly for CS07-REAS. Overall, simultaneous reductions in NO_x and VOCs decrease SIA levels in most cities, similar to the effects of NO_x controls alone.

Figure S8 shows the relative changes in SIA due to NO_x controls on a national scale, using different mechanisms and inventories. The stepwise reductions in NO_x emissions lead to an overall decrease in SIA concentrations, with the most pronounced reductions observed in the NCP, SCB, Jiangsu, Bohai Bay, and Yellow Sea. The decreases in SIA increase from ~5% to 60% as NO_x reduction increases from 20% to 80%. On the contrary, VOC reduction causes an overall increase in SIA concentrations (Figure S9), indicating that VOC controls are less effective than NO_x controls in reducing SIA levels in July. Notably, the largest increases in SIA are seen in SCB, Central, and YRD, where SIA increases grow from ~ 6% to 30% as VOC reduction increases from 20% to 80%. In comparison, S18-REAS shows relatively smaller changes in SIA, with some areas in NCP showing obvious decreases in SIA concentrations.

3.5.3 Impacts of mechanisms and inventories on OH and NO_3 sensitivity

As shown in Figures 8-9, the effects of NO_x reductions on OH concentrations vary depending on the mechanism and inventory used. In most regions, OH production decreases with reducing NO_x emissions, likely due to the decrease in O_3 concentrations, as O_3 photolysis in the presence of water vapor is a significant source of atmospheric OH (Seinfeld and Pandis, 2016). Except for Shenzhen, CS07-MEIC and CS07-REAS predict the largest decreases in OH due to NO_x control in other cities, while S18-REAS predicts the smallest OH change rates. In Shenzhen, OH levels predicted by S11-MEIC and CS07-MEIC initially increase and then decrease as NO_x emissions decrease, while those predicted by S18-REAS, CS07-REAS, and S11-REAS exhibit a consistent decrease in OH levels. When only VOCs are reduced, the changes in OH vary across different mechanisms and inventories. In Beijing, except for S18-REAS, OH concentration initially increases and then decreases with decreasing VOC emissions. In Shanghai, OH concentrations from CS07-REAS and S11-REAS basically increase with decreasing VOCs, while those from CS07-MEIC and S11-MEIC show an initial increase followed by a decrease. S18-REAS predicts a general decrease of OH with decreasing VOCs in Beijing and Shanghai. In Changsha, OH concentrations consistently increase with reduced VOCs across all mechanisms and inventories, with CS07-REAS showing a rapid increase of up to 75%. In Shenzhen, OH levels from CS07-REAS, S11-REAS, and S18-REAS increase with decreasing VOCs, while those from S11-MEIC and CS07-MEIC decrease. In Chongqing, all mechanisms and inventories except S18-REAS predict an increase in OH concentrations with decreasing VOCs, with CS07-MEIC showing a significant increase of up to 75%. When

470 both NO_x and VOC emissions are reduced, OH concentrations generally increase for all

471 mechanisms and inventories, although the relative changes are relatively small (< 25%).

472 Figures S10-S11 display the spatial distribution of OH changes due to incremental emission

473 controls across different mechanisms and inventories. There is a nationwide decrease in OH

474 concentrations due to NO_x reductions, with more pronounced decreases in central and eastern

475 China, where OH levels drop by ~ 20% to 80% as NO_x reduction increases from 20% to 80%.

476 Instead, VOC reductions generally lead to increased OH concentrations across most of China,

477 significantly in some regions with large vegetation cover (Kang et al., 2023a), such as central

478 and southeastern China. In these areas, OH levels increase by 20~200% in response to stepwise

479 VOC reductions. This increase occurs because high atmospheric VOC concentrations in rural

480 and vegetation-rich areas react with OH radicals to produce RO_2 and HO_2, depleting OH, thus

481 reducing VOCs in these areas increases OH levels. However, in some urban centers, such as

482 Beijing and Shanghai, changes in OH levels due to VOC controls depend on the extent of

483 reduction and the choice of mechanism and inventory.

484 Similar to OH, NO_3 levels predicted by different mechanisms and inventories basically

485 decrease with decreasing NO_x emissions, likely related to the decline of O_3 concentrations since

486 NO_3 radicals are predominantly formed by the reaction of NO_2 with O_3 (Geyer et al., 2001). In

487 general, the change rates of NO_3 due to NO_x reductions are higher for CS07-MEIC and CS07-

488 REAS, while lower for S18-REAS. When VOC emissions are reduced, NO_3 production

489 increases, except for S18-REAS. In Changsha, a particularly dramatic increase of over 200%

490 and 150% is observed for CS07-REAS and CS07-MEIC, respectively, when VOC emissions

491 are cut by 80%. This increase in NO_3 radicals could be attributed to a decline in the rapid

492 reaction of NO_3 with unsaturated hydrocarbons. However, for S18-REAS, NO_3 concentrations

493 decrease with decreasing VOCs in Beijing, Shanghai, and Chongqing. Unlike OH,

494 simultaneous reductions in NO_x and VOCs result in lower NO_3 levels across all mechanisms

495 and inventories.

496 Figures S12-13 illustrate the spatial variation in NO_3 changes due to systematic emission

497 reductions for all mechanisms and inventories. NO_3 radicals show a decreasing trend,

498 particularly in eastern China, where reductions in NO_3 levels vary from 40% to 100%. Except

499 for S18-REAS, other mechanisms and inventories generally predict a nationwide increase in

500 NO_3 radicals with reduced VOCs, particularly in central and southeastern China, where NO_3

501 levels increase by ~ 30 – 300% or even more with increasing VOC reductions. S18-REAS

502 predicts a decrease in NO_3 levels with reduced VOCs in some megacities such as Beijing,

503 Shanghai, Chengdu, and Chongqing, while NO_3 levels increase elsewhere.

3.5.4 Impacts of mechanisms and inventories on the sensitivity of secondary gaseous pollutants to emission controls

As shown in Figure 10, HCHO concentrations decrease with decreasing NO_x emissions, likely due to decreased AOC, as evidenced by decreased OH and NO_3 levels. This indicates that secondary formation from the oxidation of atmospheric VOCs is the dominant source of HCHO, in accordance with previous studies (Wang et al., 2017; Yang et al., 2019; Zhang et al., 2013). In addition, the most significant decreases in HCHO levels due to NO_x reductions are observed for CS07-REAS in all five cities, particularly in Changsha and Chongqing, where HCHO levels drop by about 40%. When VOCs are reduced alone, HCHO levels decrease linearly across all mechanisms and inventories, a trend similar to the simultaneous reduction of NO_x and VOCs. Variations in HCHO changes across different mechanisms and inventories suggest the need to evaluate different mechanisms and inventories when formulating regional emission control policies for carbonyl pollution.

Figures S14- S15 illustrate the spatial distribution of relative changes in HCHO due to NO_x and VOC controls using different mechanisms and inventories. VOC and NO_x controls lead to reductions in HCHO concentration, especially in eastern China. However, VOC controls generally lead to larger reductions in HCHO concentrations (~10–80%) than NO_x controls (~ 4 – 40%), as shown in Figures S14-15 and 10. This suggests that VOC controls are also essential and more effective for reducing secondary gaseous organic pollutants in the atmosphere.

4. Conclusions

This study utilized the CMAQ model to evaluate the impacts of different mechanisms and inventories on the prediction of O_3 and other air pollutants. It also examined how these mechanisms and inventories affect the sensitivity of O_3 and related species to emission reductions. For O_3-8h, relative reductions predicted using different emission inventory and mechanism combinations are consistent for up to 80% NO_x or VOC reductions, with maximum differences of approximately 15%. For SIA, while the predicted relative changes in their daily average concentrations due to NO_x reductions are quite similar, very large differences of up to 30% occur for VOC reductions. Sometimes even the direction of change (i.e., increase or decrease) is different. For the oxidants OH and NO_3 radicals, the uncertainties in the relative changes due to emission changes are even larger among different inventory-mechanism combinations, sometimes by as much as 200%. Our results suggest that while the O_3-8h

538 responses to emission changes are not sensitive to the choice of chemical mechanism and
539 emission inventories, using a single model and mechanism to evaluate the effectiveness of
540 emission controls on SIA and atmospheric oxidation capacity may have large errors. For these
541 species, the evaluation of the control strategies may require an ensemble approach with
542 multiple inventories and mechanisms.
543

544 **Data availability**. The dataset for this paper is available upon request from the corresponding
545 author (qying@ust.hk).

546 **Author contributions.** QY designed the study. QY and MJK developed the CMAQ model.
547 MJK conducted the simulations, analyzed the data, and wrote the manuscript. All coauthors
548 contributed to the discussion and revision of the paper.

549 **Competing interests**. The authors declare that they have no conflict of interest.

550 **Acknowledgments**

551 This work was partly supported by the National Natural Science Foundation of China (No.
552 42307142).

References

Akimoto, H., Ohara, T., Kurokawa, J., and Horii, N.: Verification of energy consumption in China during 1996–2003 by using satellite observational data, Atmospheric Environment, 40, 7663–7667, https://doi.org/10.1016/j.atmosenv.2006.07.052, 2006.

Boylan, J. W. and Russell, A. G.: PM and light extinction model performance metrics, goals, and criteria for three-dimensional air quality models, Atmospheric Environment, 40, 4946–4959, https://doi.org/10.1016/j.atmosenv.2005.09.087, 2006.

Bray, C. D., Strum, M., Simon, H., Riddick, L., Kosusko, M., Menetrez, M., Hays, M. D., and Rao, V.: An assessment of important SPECIATE profiles in the EPA emissions modeling platform and current data gaps, Atmospheric Environment, 207, 93–104, https://doi.org/10.1016/j.atmosenv.2019.03.013, 2019.

Byun, D. and Schere, K. L.: Review of the Governing Equations, Computational Algorithms, and Other Components of the Models-3 Community Multiscale Air Quality (CMAQ) Modeling System, Applied Mechanics Reviews, 59, 51–77, https://doi.org/10.1115/1.2128636, 2006.

Carter, W. P. L.: Development of a condensed SAPRC-07 chemical mechanism, Atmospheric Environment, 44, 5336–5345, https://doi.org/10.1016/j.atmosenv.2010.01.024, 2010.

Carter, W. P. L.: Development of a database for chemical mechanism assignments for volatile organic emissions, Journal of the Air & Waste Management Association, 65, 1171–1184, https://doi.org/10.1080/10962247.2015.1013646, 2015.

Carter, W. P. L.: Documentation of the SAPRC-18 mechansim, Report to the California Air Resources Board, 2020.

Carter, W. P. L. and Heo, G.: Development of revised SAPRC aromatics mechanisms, Atmos. Environ., 77, 404–414, https://doi.org/10.1016/j.atmosenv.2013.05.021, 2013.

Carter, W. P. L., Jiang, J., Orlando, J. J., and Barsanti, K. C.: Derivation of atmospheric reaction mechanisms for volatile organic compounds by the SAPRC mechanism generation system (MechGen), Atmospheric Chemistry and Physics, 25, 199–242, https://doi.org/10.5194/acp-25-199-2025, 2025.

Du, H., Yan, M., Liu, X., Zhong, Y., Ban, J., Lu, K., and Li, T.: Exposure to Concurrent Heatwaves and Ozone Pollution and Associations with Mortality Risk: A Nationwide Study in China, Environmental Health Perspectives, 132, 047012, https://doi.org/10.1289/EHP13790, 2024.

Elshorbany, Y. F., Kurtenbach, R., Wiesen, P., Lissi, E., Rubio, M., Villena, G., Gramsch, E., Rickard, A. R., Pilling, M. J., and Kleffmann, J.: Oxidation capacity of the city air of Santiago, Chile, Atmospheric Chemistry and Physics, 9, 2257–2273, https://doi.org/10.5194/acp-9-2257-2009, 2009.

590 Emery, C., Liu, Z., Russell, A. G., Odman, M. T., Yarwood, G., and Kumar, N.:
591 Recommendations on statistics and benchmarks to assess photochemical model
592 performance, Journal of the Air & Waste Management Association, 67, 582–598,
593 https://doi.org/10.1080/10962247.2016.1265027, 2017.

594 Feng, Z., Xu, Y., Kobayashi, K., Dai, L., Zhang, T., Agathokleous, E., Calatayud, V., Paoletti, E.,
595 Mukherjee, A., Agrawal, M., Park, R. J., Oak, Y. J., and Yue, X.: Ozone pollution threatens the
596 production of major staple crops in East Asia, Nat Food, 3, 47–56,
597 https://doi.org/10.1038/s43016-021-00422-6, 2022.

598 Finlayson-Pitts, B. J. and Pitts Jr, J. N.: Chemistry of the upper and lower atmosphere:
599 theory, experiments, and applications, Elsevier, 1999.

600 Geyer, A., Alicke, B., Konrad, S., Schmitz, T., Stutz, J., and Platt, U.: Chemistry and oxidation
601 capacity of the nitrate radical in the continental boundary layer near Berlin, Journal of
602 Geophysical Research: Atmospheres, 106, 8013–8025,
603 https://doi.org/10.1029/2000JD900681, 2001.

604 Ghude, S. D., Chate, D. M., Jena, C., Beig, G., Kumar, R., Barth, M. C., Pfister, G. G., Fadnavis,
605 S., and Pithani, P.: Premature mortality in India due to PM2.5 and ozone exposure,
606 Geophysical Research Letters, 43, 4650–4658, https://doi.org/10.1002/2016GL068949,
607 2016.

608 Griffith, S. M., Hansen, R. F., Dusanter, S., Michoud, V., Gilman, J. B., Kuster, W. C., Veres, P.
609 R., Graus, M., de Gouw, J. A., Roberts, J., Young, C., Washenfelder, R., Brown, S. S., Thalman,
610 R., Waxman, E., Volkamer, R., Tsai, C., Stutz, J., Flynn, J. H., Grossberg, N., Lefer, B., Alvarez,
611 S. L., Rappenglueck, B., Mielke, L. H., Osthoff, H. D., and Stevens, P. S.: Measurements of
612 hydroxyl and hydroperoxy radicals during CalNex-LA: Model comparisons and radical
613 budgets, Journal of Geophysical Research: Atmospheres, 121, 4211–4232,
614 https://doi.org/10.1002/2015JD024358, 2016.

615 Hu, J., Li, X., Huang, L., Ying, Q., Zhang, Q., Zhao, B., Wang, S., and Zhang, H.: Ensemble
616 prediction of air quality using the WRF/CMAQ model system for health effect studies in
617 China, Atmospheric Chemistry and Physics, 17, 13103–13118, https://doi.org/10.5194/acp-
618 17-13103-2017, 2017a.

619 Hu, J., Huang, L., Chen, M., Liao, H., Zhang, H., Wang, S., Zhang, Q., and Ying, Q.: Premature
620 Mortality Attributable to Particulate Matter in China: Source Contributions and Responses
621 to Reductions, Environ. Sci. Technol., 51, 9950–9959,
622 https://doi.org/10.1021/acs.est.7b03193, 2017b.

623 Jiang, J., Carter, W. P. L., Cocker, D. R. I., and Barsanti, K. C.: Development and Evaluation of
624 a Detailed Mechanism for Gas-Phase Atmospheric Reactions of Furans, ACS Earth Space
625 Chem., 4, 1254–1268, https://doi.org/10.1021/acsearthspacechem.0c00058, 2020.

626 Kang, M., Zhang, J., Zhang, H., and Ying, Q.: On the Relevancy of Observed Ozone Increase
627 during COVID-19 Lockdown to Summertime Ozone and PM2.5 Control Policies in China,
628 Environ. Sci. Technol. Lett., 8, 289–294, https://doi.org/10.1021/acs.estlett.1c00036, 2021.

629   Kang, M., Hu, J., Zhang, H., and Ying, Q.: Evaluation of a highly condensed SAPRC chemical
630   mechanism and two emission inventories for ozone source apportionment and emission
631   control strategy assessments in China, Science of The Total Environment, 813, 151922,
632   https://doi.org/10.1016/j.scitotenv.2021.151922, 2022.

633   Kang, M., Zhang, H., and Ying, Q.: Enhanced summertime background ozone by
634   anthropogenic emissions – Implications on ozone control policy and health risk assessment,
635   Atmospheric Environment, 314, 120116, https://doi.org/10.1016/j.atmosenv.2023.120116,
636   2023a.

637   Kang, M., Zhang, H., and Ying, Q.: Enhanced summertime background ozone by
638   anthropogenic emissions – Implications on ozone control policy and health risk assessment,
639   Atmospheric Environment, 120116, https://doi.org/10.1016/j.atmosenv.2023.120116,
640   2023b.

641   Kim, Y., Sartelet, K., and Seigneur, C.: Comparison of two gas-phase chemical kinetic
642   mechanisms of ozone formation over Europe, J Atmos Chem, 62, 89–119,
643   https://doi.org/10.1007/s10874-009-9142-5, 2009.

644   Lei, Y., Zhang, Q., He, K. B., and Streets, D. G.: Primary anthropogenic aerosol emission
645   trends for China, 1990–2005, Atmospheric Chemistry and Physics, 11, 931–954,
646   https://doi.org/10.5194/acp-11-931-2011, 2011.

647   Li, J., Zhang, H., and Ying, Q.: Comparison of the SAPRC07 and SAPRC99 photochemical
648   mechanisms during a high ozone episode in Texas: Differences in concentrations, OH budget
649   and relative response factors, Atmospheric Environment, 54, 25–35,
650   https://doi.org/10.1016/j.atmosenv.2012.02.034, 2012.

651   Li, K., Jacob, D. J., Liao, H., Shen, L., Zhang, Q., and Bates, K. H.: Anthropogenic drivers of
652   2013–2017 trends in summer surface ozone in China, Proc Natl Acad Sci USA, 116, 422–427,
653   https://doi.org/10.1073/pnas.1812168116, 2019.

654   Li, K., Zhang, X., Zhao, B., Bloss, W. J., Lin, C., White, S., Yu, H., Chen, L., Geng, C., Yang, W.,
655   Azzi, M., George, C., and Bai, Z.: Suppression of anthropogenic secondary organic aerosol
656   formation by isoprene, npj Clim Atmos Sci, 5, 1–9, https://doi.org/10.1038/s41612-022-
657   00233-x, 2022a.

658   Li, M., Zhang, Q., Streets, D. G., He, K. B., Cheng, Y. F., Emmons, L. K., Huo, H., Kang, S. C., Lu,
659   Z., Shao, M., Su, H., Yu, X., and Zhang, Y.: Mapping Asian anthropogenic emissions of non-
660   methane volatile organic compounds to multiple chemical mechanisms, Atmospheric
661   Chemistry and Physics, 14, 5617–5638, https://doi.org/10.5194/acp-14-5617-2014, 2014.

662   Li, N., He, Q., Greenberg, J., Guenther, A., Li, J., Cao, J., Wang, J., Liao, H., Wang, Q., and
663   Zhang, Q.: Impacts of biogenic and anthropogenic emissions on summertime ozone
664   formation in the Guanzhong Basin, China, Atmospheric Chemistry and Physics, 18, 7489–
665   7507, https://doi.org/10.5194/acp-18-7489-2018, 2018.

666   Li, Q., Jiang, J., Afreh, I. K., Barsanti, K. C., and Cocker III, D. R.: Secondary organic aerosol
667   formation from camphene oxidation: measurements and modeling, Atmospheric Chemistry
668   and Physics, 22, 3131–3147, https://doi.org/10.5194/acp-22-3131-2022, 2022b.

669   Liu, T., Hong, Y., Li, M., Xu, L., Chen, J., Bian, Y., Yang, C., Dan, Y., Zhang, Y., Xue, L., Zhao, M.,
670   Huang, Z., and Wang, H.: Atmospheric oxidation capacity and ozone pollution mechanism in
671   a coastal city of southeastern China: analysis of a typical photochemical episode by an
672   observation-based model, Atmospheric Chemistry and Physics, 22, 2173–2190,
673   https://doi.org/10.5194/acp-22-2173-2022, 2022.

674   Lu, X., Hong, J., Zhang, L., Cooper, O. R., Schultz, M. G., Xu, X., Wang, T., Gao, M., Zhao, Y.,
675   and Zhang, Y.: Severe surface ozone pollution in China: A global perspective, Environmental
676   Science & Technology Letters, 5, 487–494, 2018.

677   Lu, X., Zhang, L., Wang, X., Gao, M., Li, K., Zhang, Y., Yue, X., and Zhang, Y.: Rapid Increases in
678   Warm-Season Surface Ozone and Resulting Health Impact in China Since 2013, Environ. Sci.
679   Technol. Lett., 7, 240–247, https://doi.org/10.1021/acs.estlett.0c00171, 2020.

680   Luhar, A. K., Galbally, I. E., Woodhouse, M. T., and Thatcher, M.: An improved
681   parameterisation of ozone dry deposition to the ocean and its impact in a global climate–
682   chemistry model, Atmos. Chem. Phys., 17, 3749–3767, https://doi.org/10.5194/acp-17-
683   3749-2017, 2017.

684   Lyu, X., Li, K., Guo, H., Morawska, L., Zhou, B., Zeren, Y., Jiang, F., Chen, C., Goldstein, A. H.,
685   Xu, X., Wang, T., Lu, X., Zhu, T., Querol, X., Chatani, S., Latif, M. T., Schuch, D., Sinha, V.,
686   Kumar, P., Mullins, B., Seguel, R., Shao, M., Xue, L., Wang, N., Chen, J., Gao, J., Chai, F.,
687   Simpson, I., Sinha, B., and Blake, D. R.: A synergistic ozone-climate control to address
688   emerging ozone pollution challenges, One Earth, 6, 964–977,
689   https://doi.org/10.1016/j.oneear.2023.07.004, 2023.

690   Ma, J. and van Aardenne, J. A.: Impact of different emission inventories on simulated
691   tropospheric ozone over China: a regional chemical transport model evaluation,
692   Atmospheric Chemistry and Physics, 4, 877–887, https://doi.org/10.5194/acp-4-877-2004,
693   2004.

694   Placet, M., Mann, C. O., Gilbert, R. O., and Niefer, M. J.: Emissions of ozone precursors from
695   stationary sources:: a critical review, Atmospheric Environment, 34, 2183–2204,
696   https://doi.org/10.1016/S1352-2310(99)00464-1, 2000.

697   Prinn, R. G.: The Cleansing Capacity of the Atmosphere, Annual Review of Environment and
698   Resources, 28, 29–57, https://doi.org/10.1146/annurev.energy.28.011503.163425, 2003.

699   Real, E., Megaritis, A., Colette, A., Valastro, G., and Messina, P.: Atlas of ozone chemical
700   regimes in Europe, Atmospheric Environment, 320, 120323,
701   https://doi.org/10.1016/j.atmosenv.2023.120323, 2024.

702   Russell, A.: REGIONAL PHOTOCHEMICAL AIR QUALITY MODELING:Model Formulations,
703   History, and State of the Science, Annual Review of Environment and Resources, 22, 537–
704   588, https://doi.org/10.1146/annurev.energy.22.1.537, 1997.

705   Saikawa, E., Kim, H., Zhong, M., Avramov, A., Zhao, Y., Janssens-Maenhout, G., Kurokawa, J.,
706   Klimont, Z., Wagner, F., Naik, V., Horowitz, L. W., and Zhang, Q.: Comparison of emissions
707   inventories of anthropogenic air pollutants and greenhouse gases in China, Atmospheric
708   Chemistry and Physics, 17, 6393–6421, https://doi.org/10.5194/acp-17-6393-2017, 2017.

709   Seinfeld, J. H. and Pandis, S. N.: Atmospheric Chemistry and Physics: From Air Pollution to
710   Climate Change, John Wiley & Sons, 1152 pp., 2016.

711   Sha, Q., Zhu, M., Huang, H., Wang, Y., Huang, Z., Zhang, X., Tang, M., Lu, M., Chen, C., Shi, B.,
712   Chen, Z., Wu, L., Zhong, Z., Li, C., Xu, Y., Yu, F., Jia, G., Liao, S., Cui, X., Liu, J., and Zheng, J.: A
713   newly integrated dataset of volatile organic compounds (VOCs) source profiles and
714   implications for the future development of VOCs profiles in China, Science of The Total
715   Environment, 793, 148348, https://doi.org/10.1016/j.scitotenv.2021.148348, 2021.

716   Silva, S. J. and Heald, C. L.: Investigating Dry Deposition of Ozone to Vegetation, Journal of
717   Geophysical Research: Atmospheres, 123, 559–573,
718   https://doi.org/10.1002/2017JD027278, 2018.

719   Streets, D. G., Bond, T. C., Carmichael, G. R., Fernandes, S. D., Fu, Q., He, D., Klimont, Z.,
720   Nelson, S. M., Tsai, N. Y., Wang, M. Q., Woo, J.-H., and Yarber, K. F.: An inventory of gaseous
721   and primary aerosol emissions in Asia in the year 2000, Journal of Geophysical Research:
722   Atmospheres, 108, https://doi.org/10.1029/2002JD003093, 2003.

723   Wang, C., Huang, X.-F., Han, Y., Zhu, B., and He, L.-Y.: Sources and Potential Photochemical
724   Roles of Formaldehyde in an Urban Atmosphere in South China, Journal of Geophysical
725   Research: Atmospheres, 122, 11,934-11,947, https://doi.org/10.1002/2017JD027266, 2017.

726   Wang, P., Ying, Q., Zhang, H., Hu, J., Lin, Y., and Mao, H.: Source apportionment of
727   secondary organic aerosol in China using a regional source-oriented chemical transport
728   model and two emission inventories, Environmental Pollution, 237, 756–766,
729   https://doi.org/10.1016/j.envpol.2017.10.122, 2018.

730   West, J. J., Fiore, A. M., Horowitz, L. W., and Mauzerall, D. L.: Global health benefits of
731   mitigating ozone pollution with methane emission controls, Proceedings of the National
732   Academy of Sciences of the United States of America, 103, 3988,
733   https://doi.org/10.1073/pnas.0600201103, 2006.

734   Wiedinmyer, C., Akagi, S. K., Yokelson, R. J., Emmons, L. K., Al-Saadi, J. A., Orlando, J. J., and
735   Soja, A. J.: The Fire INventory from NCAR (FINN): a high resolution global model to estimate
736   the emissions from open burning, Geoscientific Model Development, 4, 625–641,
737   https://doi.org/10.5194/gmd-4-625-2011, 2011.

738   Wu, R. and Xie, S.: Spatial Distribution of Ozone Formation in China Derived from Emissions
739   of Speciated Volatile Organic Compounds, Environ. Sci. Technol., 51, 2574–2583,
740   https://doi.org/10.1021/acs.est.6b03634, 2017.

741   Xue, T., Zheng, Y., Geng, G., Xiao, Q., Meng, X., Wang, M., Li, X., Wu, N., Zhang, Q., and Zhu,
742   T.: Estimating Spatiotemporal Variation in Ambient Ozone Exposure during 2013–2017

743   Using a Data-Fusion Model, Environ. Sci. Technol., 54, 14877–14888,
744   https://doi.org/10.1021/acs.est.0c03098, 2020.

745   Yamaji, K., Ohara, T., Uno, I., Kurokawa, J., Pochanart, P., and Akimoto, H.: Future prediction
746   of surface ozone over east Asia using models-3 community multiscale air quality modeling
747   system and regional emission inventory in Asia, Journal of Geophysical Research:
748   Atmospheres, 113, 2008.

749   Yang, Z., Cheng, H. R., Wang, Z. W., Peng, J., Zhu, J. X., Lyu, X. P., and Guo, H.: Chemical
750   characteristics of atmospheric carbonyl compounds and source identification of
751   formaldehyde in Wuhan, Central China, Atmospheric Research, 228, 95–106,
752   https://doi.org/10.1016/j.atmosres.2019.05.020, 2019.

753   Zhang, H., Li, J., Ying, Q., Guven, B. B., and Olaguer, E. P.: Source apportionment of
754   formaldehyde during TexAQS 2006 using a source-oriented chemical transport model,
755   Journal of Geophysical Research: Atmospheres, 118, 1525–1535,
756   https://doi.org/10.1002/jgrd.50197, 2013.

757   Zhang, K., Duan, Y., Huo, J., Huang, L., Wang, Y., Fu, Q., Wang, Y., and Li, L.: Formation
758   mechanism of HCHO pollution in the suburban Yangtze River Delta region, China: A box
759   model study and policy implementations, Atmospheric Environment, 267, 118755,
760   https://doi.org/10.1016/j.atmosenv.2021.118755, 2021.

761
762

763
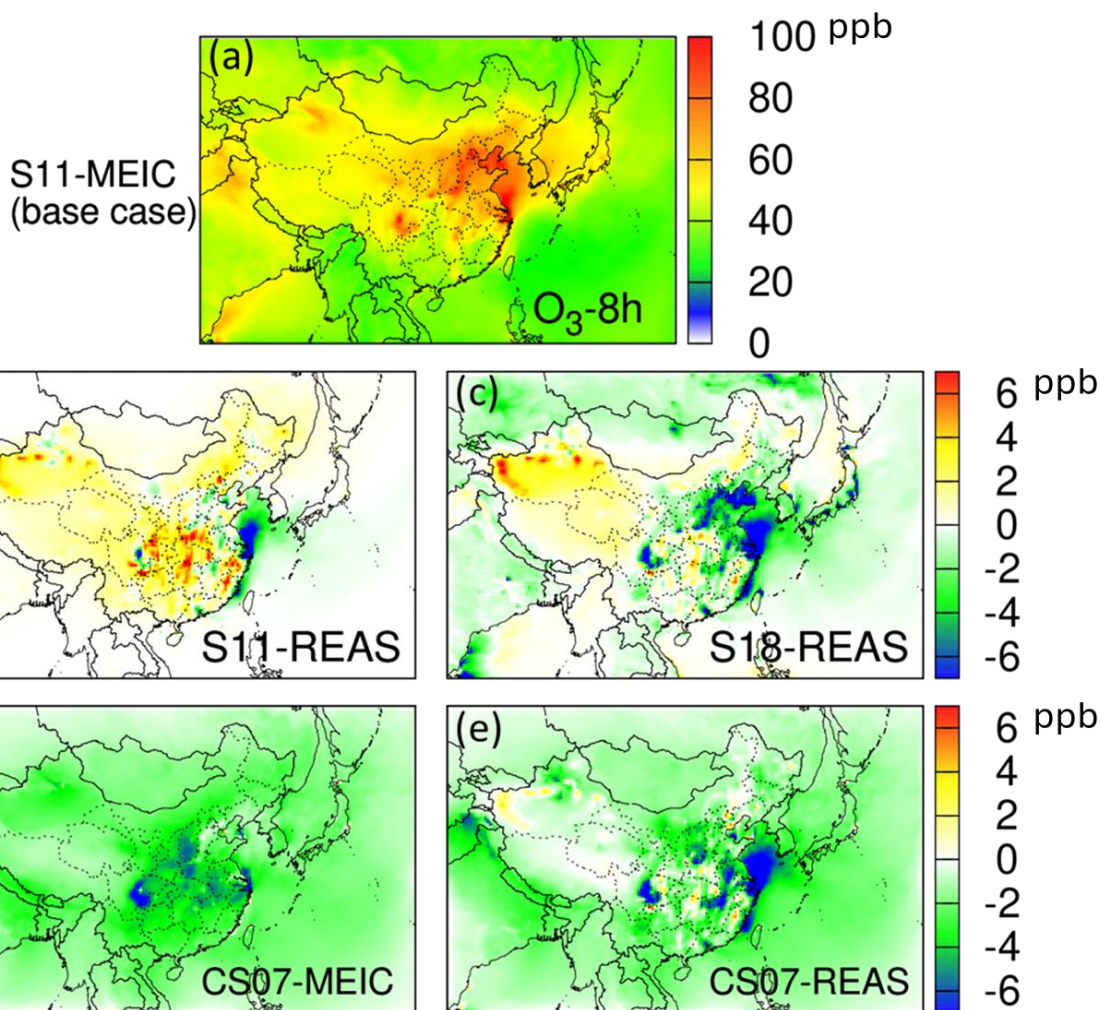
Figure 1. Predicted monthly averages of MDA8 O_3 (O_3-8h) concentrations in July 2017 using (a) the S11 mechanism and MEIC emission inventory (base case), and the differences between the base case and cases using alternative photochemical mechanisms and emission inventories (alternative case – base case): (b) S11 and REAS, (c) S18 and REAS, (d) CS07 and MEIC, and (e) CS07 and REAS inventories. Units are ppb.
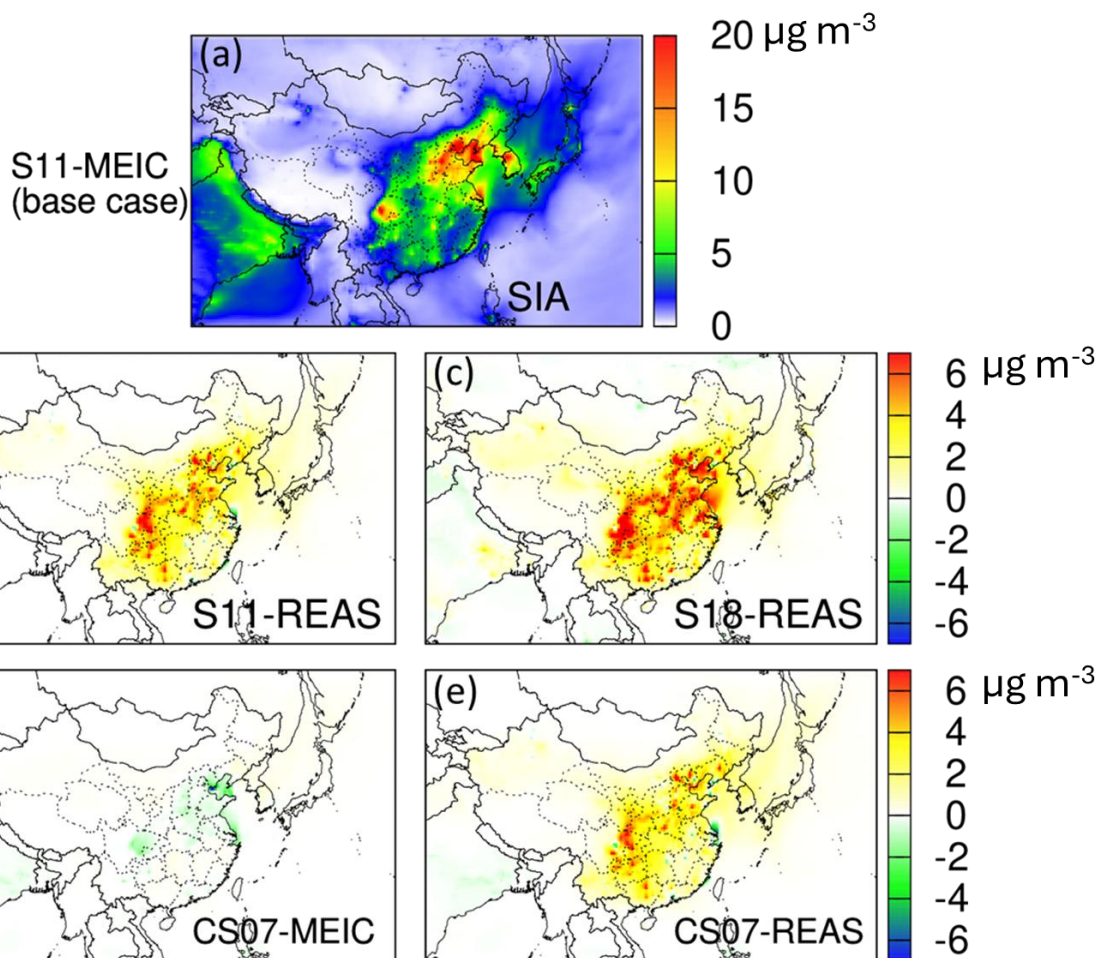
Figure 2. Predicted monthly averages of secondary inorganic aerosol (the sum of nitrate, sulfate and ammonium ion, SIA) concentrations in July 2017 using (a) the S11 mechanism and MEIC emission inventory (base case), and the differences between base case and cases using other photochemical mechanisms and emission inventories (alternative case – base case): (b) S11 and REAS, (c) S18 and REAS, (d) CS07 and MEIC, and (e) CS07 and REAS. Units are $\mu g\ m^{-3}$.
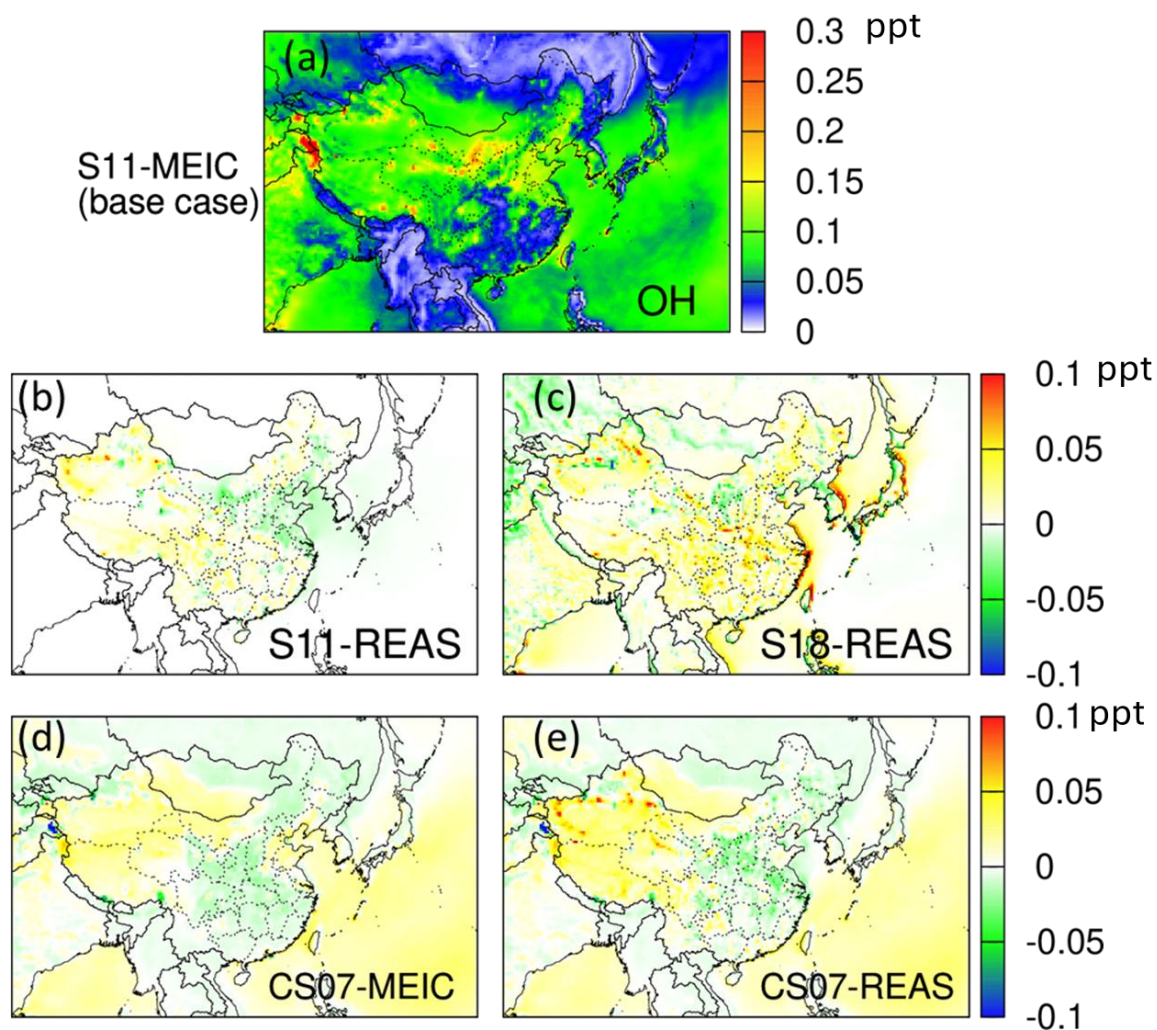
Figure 3. Predicted monthly averages of OH radical concentrations in July 2017 using (a) the S11 mechanism and MEIC emission inventory (base case), and the differences between the base case and cases using other photochemical mechanisms and emission inventories (alternative case – base case): (b) S11 and REAS, (c) S18 and REAS, (d) CS07 and MEIC, and (e) CS07 and REAS. Units are ppt. (0.1 ppt ~ 2.46×10^6 molec cm^{-3})
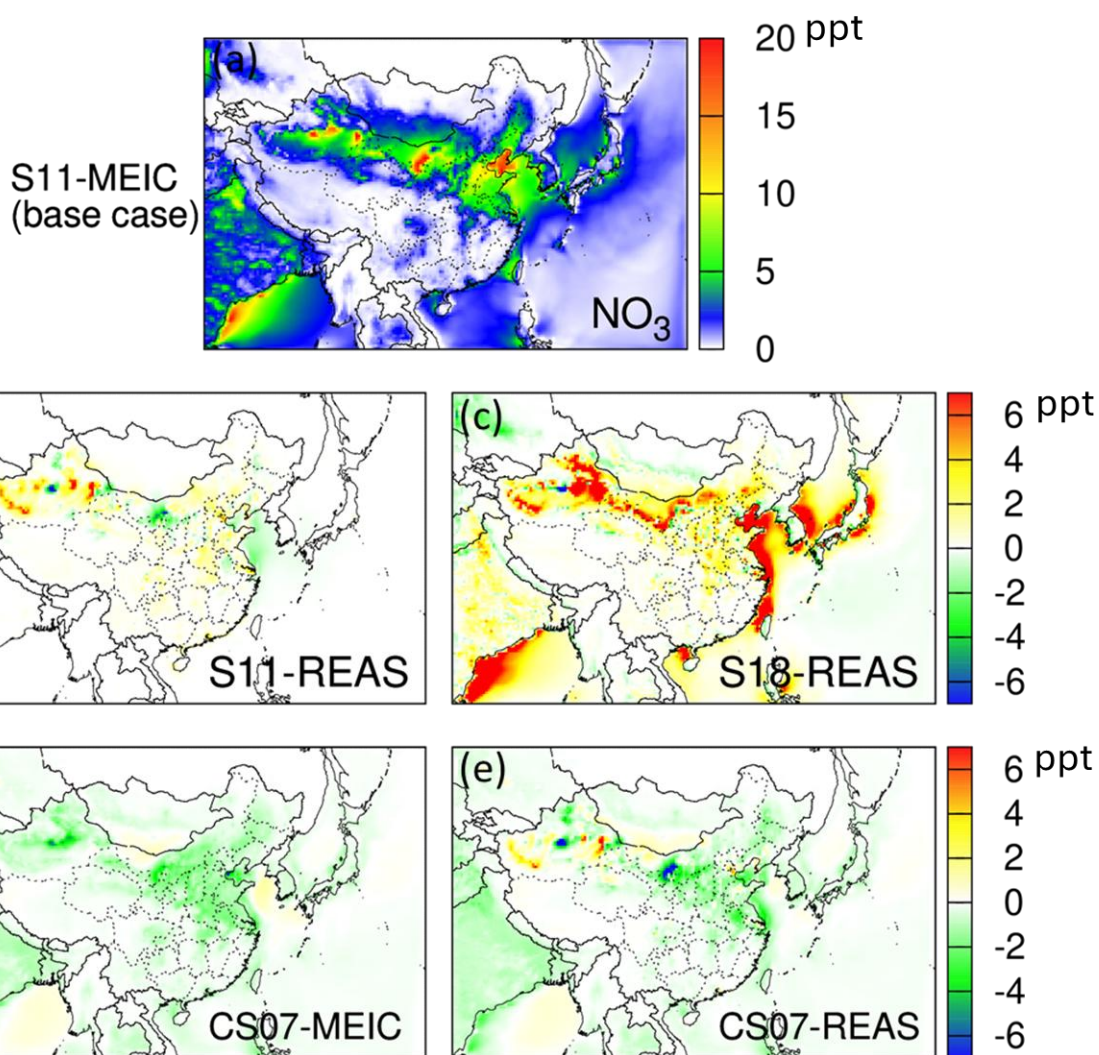
Figure 4. Predicted monthly averages of NO$_3$ radical concentrations in July 2017 using (a) the S11 mechanism and MEIC emission inventory (base case), and the differences between the base case and cases using alternative photochemical mechanisms and emission inventories (alternative case – base case): (b) S11 and REAS, (c) S18 and REAS, (d) CS07 and MEIC, and (e) CS07 and REAS. Units are in ppt. (0.1 ppt ~ 2.46×10^6 molec cm^{-3})
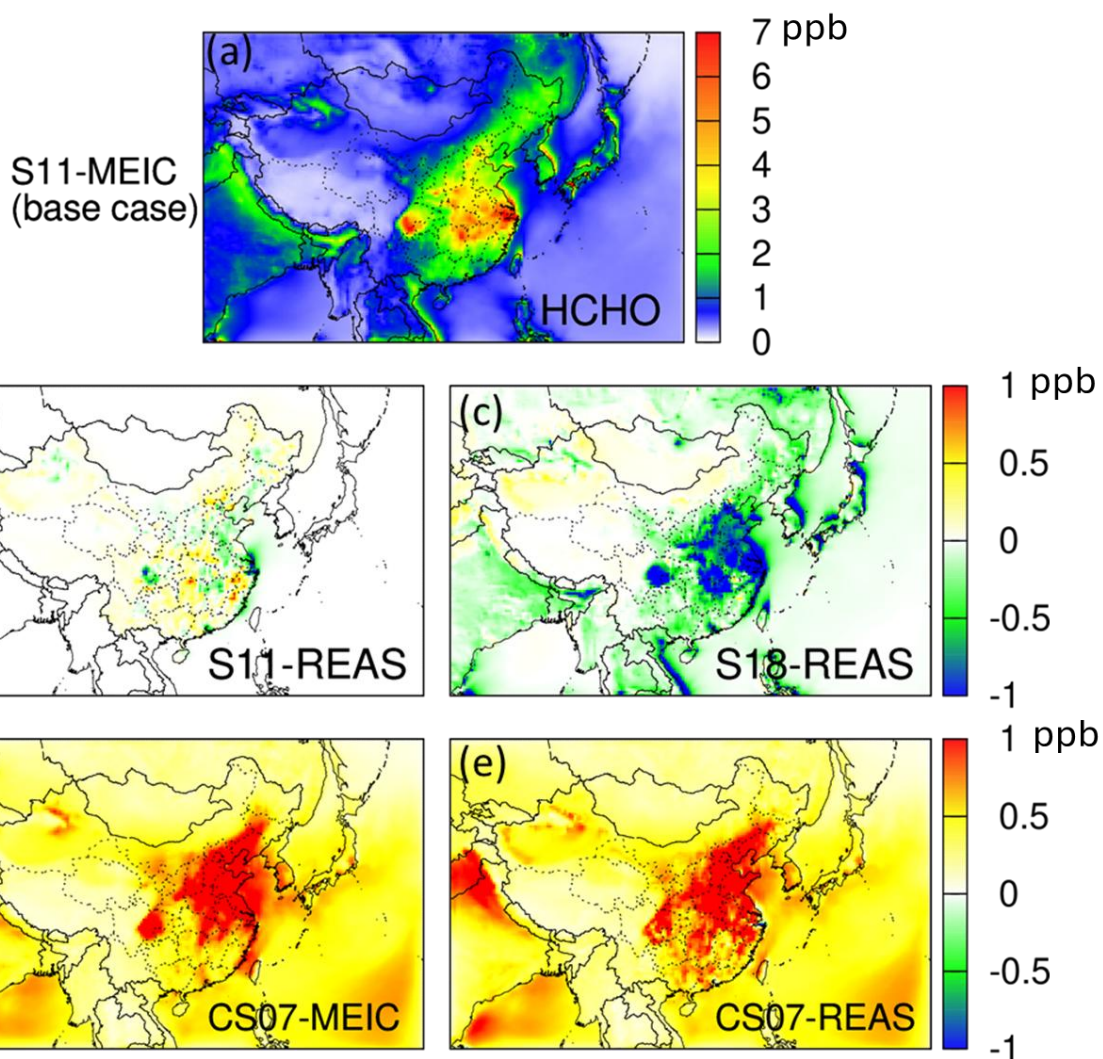
Figure 5. Predicted monthly averages of HCHO concentrations in July 2017 using (a) the S11 mechanism and MEIC emission inventory (base case), and the differences between the base case and cases using alternative photochemical mechanisms and emission inventories (alternative case – base case): (b) S11 and REAS, (c) S18 and REAS, (d) CS07 and MEIC, and (e) CS07 and REAS. Units are ppb.

799

800

801

802

803

804

805

806

807

808

809

810

811

812

813

814
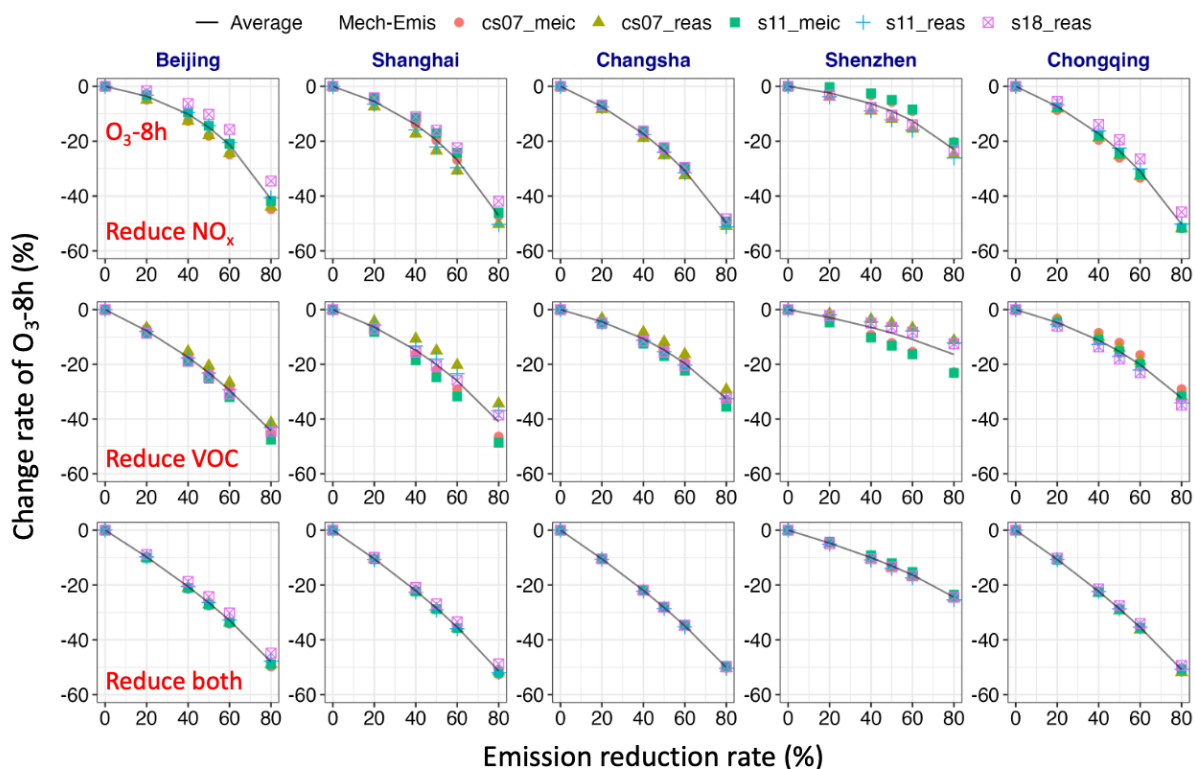
Figure 6. Predicted changes of monthly average MDA8 O_3 (O_3-8h) concentrations in July 2017 due to reductions of NO_x only (first row), VOCs only (second row), and NO_x and VOCs (third row) using different photochemical mechanisms and emission inventories. The black line represents the average change across all mechanisms and inventories at different levels of emission reductions.
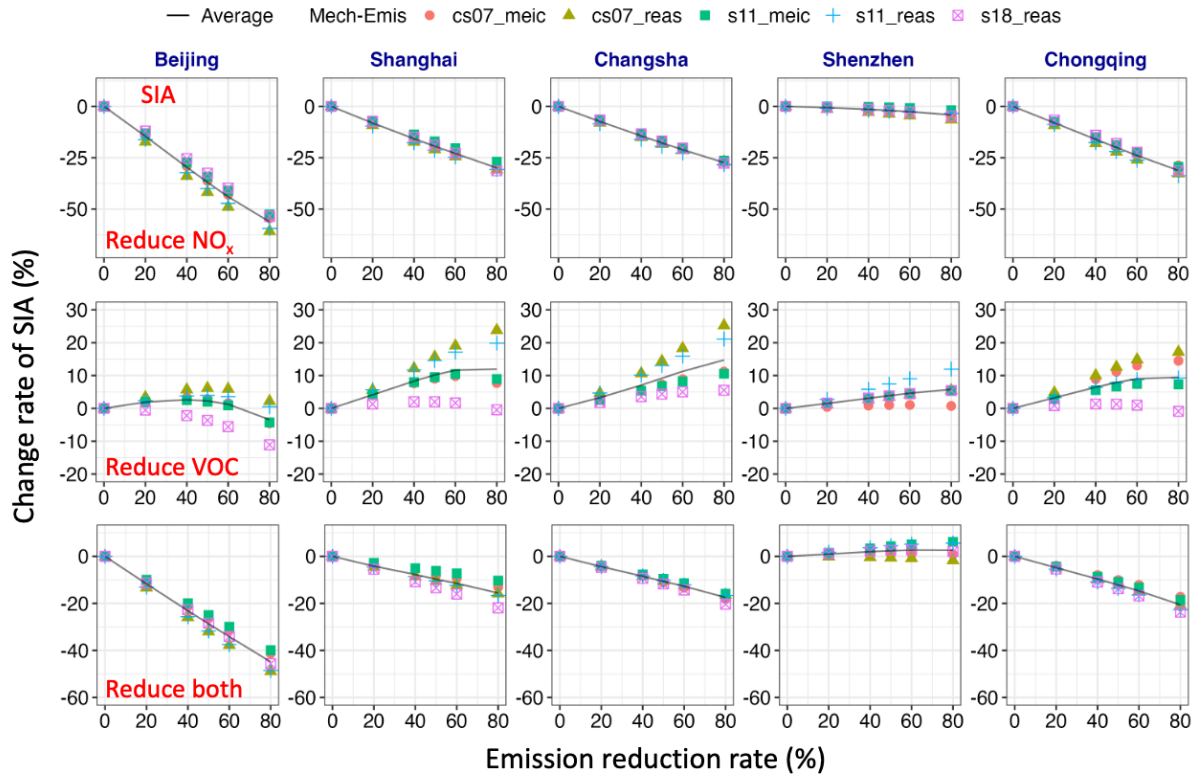
Figure 7. Predicted changes of monthly average secondary inorganic aerosol (nitrate, sulfate, and ammonium, SIA) concentrations in July 2017 due to reductions of NO$_x$ only (first row), VOCs only (second row), and NO$_x$ and VOCs (third row) using different photochemical mechanisms and emission inventories. The black line represents the average change across all mechanisms and inventories at different levels of emission reductions.
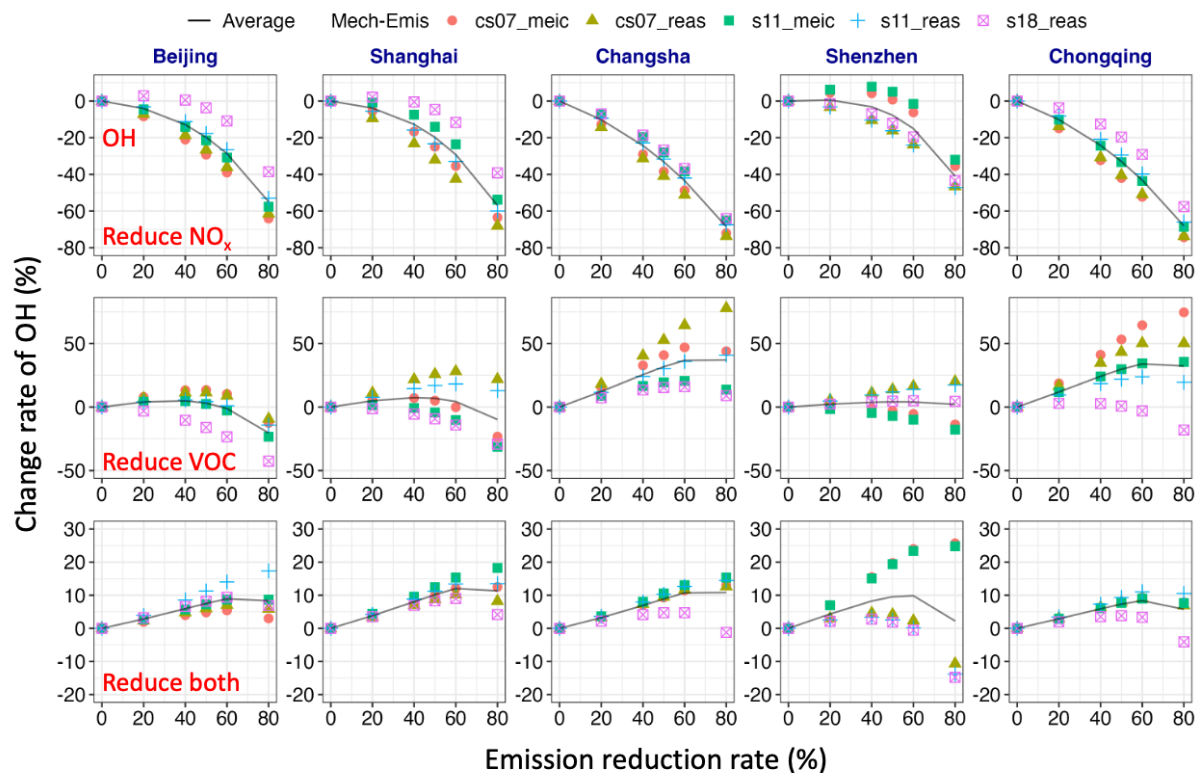
Figure 8. Predicted changes of monthly average OH radical concentrations in July 2017 due to reductions of NO_x only (first row), VOCs only (second row), and NO_x and VOCs (third row) using different photochemical mechanisms and emission inventories. The black line represents the average change across all mechanisms and inventories at different levels of emission reductions.
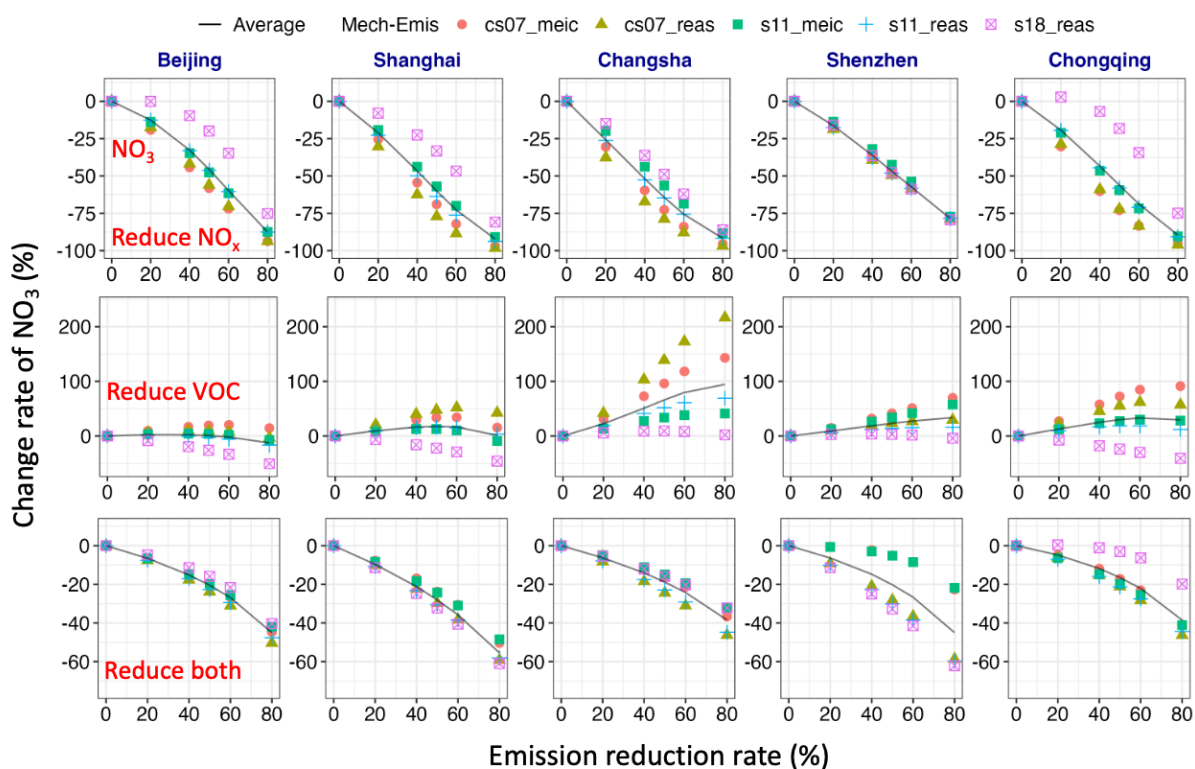
Figure 9. Predicted changes of monthly average NO$_3$ radical concentrations in July 2017 due to reductions of NO$_x$ only (first row), VOCs only (second row), and NO$_x$ and VOCs (third row) using different photochemical mechanisms and emission inventories. The black line represents the average change across all mechanisms and inventories at different levels of emission reductions.
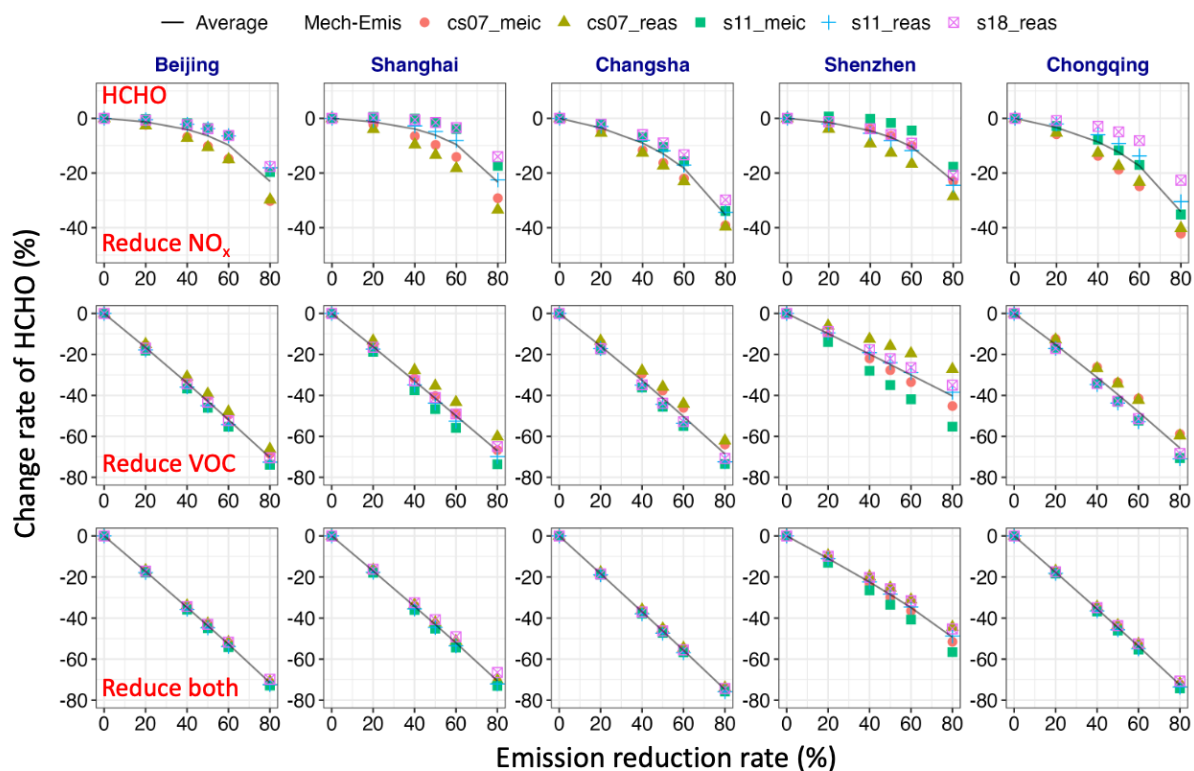
Figure 10. Predicted changes of monthly average HCHO concentrations in July 2017 due to reductions of NO_x only (first row), VOCs only (second row), and NO_x and VOCs (third row) using different photochemical mechanisms and emission inventories. The black line represents the average change across all mechanisms and inventories at different levels of emission reductions.